JMEPEG (2023) 32:2735–2748
https://doi.org/10.1007/s11665-022-07570-1



TECHNICAL ARTICLE

# Tribological Parameters Optimization of AZ31-SiC Composite Using Whale Optimization Algorithm

*Kothuri Chenchu Kishor Kumar, Bandalamudi Raghu Kumar, and Nalluri Mohan Rao*

Submitted: 20 December 2021 / Revised: 15 September 2022 / Accepted: 14 October 2022 / Published online: 23 November 2022

**In this paper, a Whale Optimization Algorithm (WOA) is proposed for the optimization of tribological parameters of AZ31-SiC metal matrix composite. Experiments were carried out by the surface of pin with the different loads of 10, 20, 30 N, velocities of 0.5, 1.0, 1.5 m $s^{-1}$ and sliding distances of 500 m, 750 m, 1000 m respectively for optimization. The equations derived from the regression analysis are considered as objective functions to find the optimal parameters of wear and coefficients of friction (COF) using WOA. Considering these objective functions, the WOA is used to optimize the tribological parameters. The optimized parameters obtained from the WOA are compared with the parameters derived from PSO, DE, FFA and experimental results. The optimum wear values obtained from WOA, PSO, DE, FFA and experiment results are 3.55, 3.63, 3.60, 3.57 and 3.77 mg respectively. The optimum values of COF obtained from WOA, PSO, DE, FFA and experiment results are 0.311, 0.313, 0.314, 0.312, and 0.33 respectively. The optimum wear values obtained from WOA, PSO, DE and FFA are 6.01, 3.89, 4.69, 5.48% lower than the experimental value. The optimum COF values obtained from WOA, PSO, DE and FFA are 5.76, 5.15, 4.85, 5.45% lower than the experimental value. It is evidence from the results that WOA has provided the best wear and COF values for AZ31-SiC metal matrix composite when compared to other methods. This proposed method reduces the time and effort of the manufacturer to use the composite material in an application with the optimum operating condition for more life. The microstructural SEM micrographs reveal the distribution of reinforcement in the composite. The SEM micrographs of worn out surfaces present various wear mechanisms of the composites under variety of operating conditions.**

**Keywords** AZ31 alloy, regression analysis, SiC reinforcement, SEM, whale optimization algorithm, wear properties

## 1. Introduction

Magnesium (Mg) and its alloys were created in response to the growing demand for lightweight materials in transportation and aerospace components (Ref 1). The weight of lever used control system of ILX-27 helicopter designed by the Institute of Aviation (Poland), fabricated by AZ31 alloy (207 g) is 35% lower than the lever fabricated by PA7 aluminium alloy (321 g) (Ref 2). There is a considerable reduction in the weight of the engine parts, nearly 35% by replacing the parts manufactured with aluminium based alloy with magnesium based alloy (Ref 3). Unfortunately, the processing qualities of magnesium, such as low hardness, strength, and poor wear resistance, limit its vast range of uses. Because of the unique working environment of particular vehicle parts (gear, bearing, or sliding sealing materials), Mg materials must not only be strong, stiff, and heat resistant, but also wear resistant. As a result, magnesium alloys may not be the best material for wear-resistant applications. As the demand for lightweight materials in the automobile sector grows, the material's friction and wear properties must be improved. The interface of matrix/reinforcement is free of cracks, porosity and cavities indicating that good wettability of SiC particle by Magnesium (Ref 4). The silicon reacts with magnesium and forms an intermetallic compound with Mg2Si which is extensively used in the automotive and aerospace industries due to its excellent mechanical, thermal, electrochemical and tribological properties (Ref 5). The wear resistance of magnesium based composites has been improved to avoid wear failures of components (Ref 6). Nano particles have a number of unique features, including isotropy, strong mechanical and wear resistance, and high-temperature inertness, making ceramic particles ideal candidates for magnesium matrix composites. In comparison to pure magnesium, adding feldspar particles to the magnesium matrix increased hardness, strength, and wear resistance (Ref 7). The wear behaviour of SiCp /AZ91 composites under high sliding speeds and normal loads, implying that the wear mechanism map was developed by observing several wear zones (Ref 8). They demonstrated that delamination wear dominated the composite wear rate. The effect of nano-Al2O3 on the wear resistance of Mg and AZ31 under various conditions like speeds and loads, indicating that abrasive and oxidative wear play major roles in the composite abrasion mechanism was studied (Ref 9, 10). The dry wear

This invited article is part of a special topical focus in the *Journal of Materials Engineering and Performance* on Magnesium. The issue was organized by Prof. C. (Ravi) Ravindran, Dr. Raja Roy, Mr. Payam Emadi, and Mr. Bernoulli Andilab, Ryerson University.

**Kothuri Chenchu Kishor Kumar**, Gudlavalleru Engineering College, Gudlavalleru, Andhra Pradesh 521356, India; **Bandalamudi Raghu Kumar**, Pradad V Potluri Siddhartha Institute of Technology, Vijayawada, Andhra Pradesh, India; and **Nalluri Mohan Rao**, Jawaharlal Nehru Technological University Kakinada, Kakinada, Andhra Pradesh, India. Contact e-mail: kchkk9874@gmail.com.

behaviour and various wear mechanisms like abrasion, adhesion, plastic deformation and wear maps for AM60B magnesium alloy (Ref 11), AM50B magnesium alloy (Ref 12) and ZE41A magnesium alloy (Ref 13) are discussed. The wear and friction behaviour of AZ31 alloy reinforced with nano SiC particles was discussed (Ref 14). In this, achieving homogeneous distribution reinforcement in the matrix and homogeneous microstructure are the issues in the fabrication of nano SiCp—reinforced composites, despite the abrasion-resistant improvement described in the aforementioned research. The effect of particle size of SiC on wear behavior with increase load for AZ91 alloy was discussed and also reported different wear mechanism with increase in load (Ref 15). Distinguished researchers from around the world used several magnesium alloys to fabricate metal matrix composites reinforced with SiC, and used multi-criteria decision making optimization to conduct numerous performance assessments. More magnesium alloys, as well as new optimization methods, remain unexploited. This study looks into the manufacture of magnesium alloy AZ31 metal matrix composite enhanced with SiC via stir casting. Control factors such as load, speed and sliding distance are used for optimization of wear and COF by Taguchi, ANOVA and regression analysis with full factorial design of experiments. Output answers included the regression equations for wear and COF.

The techniques discussed so far are complex, tedious, and consume more computational time. In order to overcome the mentioned drawbacks, in recent decades, heuristic algorithms have evolved as powerful research tools to solve many complex engineering problems in the field of science and technology. These algorithms have proven their potentiality in many complex problems for optimization, minimization of cost, and reducing the computational burden. Some of such techniques for the optimization of tribological parameters of composites are discussed hereafter. The wear characteristics of silicon nitride and hexagonal boron nitride composites using Taguchi and the simulated annealing method are presented (Ref 16). The optimization of machining parameters using simulated annealing and pattern search is addressed in (Ref 17). The methodology for the ant lion optimization algorithm was proposed (Ref 18). The optimisation of wear for aluminum alloy with SiC-Gr reinforcements was discussed by using the antlion algorithm (Ref 19). A multi-objective optimization algorithm for solving engineering problems by using an Ant lion optimizing algorithm was reported (Ref 20). They also discussed the determination of optimum wear using the algorithm in comparison with the value obtained from experimental analysis. An application of genetic algorithm was used to optimize the process parameters of Al Matrix nano composites were discussed in (Ref 21). A hybrid PSO-GA algorithm for optimization of laminated composites was discussed (Ref 22). The forecast of grinding temperature at high speed for titanium composites by using the PSO algorithm was discussed (Ref 23). The computational methods and optimization of machining parameters of composites using PSO were reported (Ref 24). A differential evolution algorithm was used to design a compliant micro gripper (Ref 25). A Differential evolution algorithm was used for the optimization of milling parameters for AISI 1050 steel (Ref 26). The process parameters optimization for friction stir welding was done by using a differential evolution algorithm (Ref 27). The process of using the firefly algorithm to solve non-linear design problems such as optimisation of standard pressure vessel design was discussed (Ref 28). Though they have provided better results, the above techniques require a greater number of design parameters and steps for the optimization process. In recent years, WOA and improved WOA have been identified as the prominent algorithm which requires a very small number of design parameters and steps to optimize the design parameters (Ref 29-31).

Hence, in this paper, a method is proposed for the optimization of tribological parameters of AZ31-SiC metal matrix composite using WOA. The regression equations for wear and COF are considered as the objective functions to find the optimum values of wear and COF using the proposed WOA. The performance of the WOA is also compared with experiment values and other algorithms like PSO, DE, and FFA.

The rest of the paper is followed as follows: the second section describes the methodology carried out in this paper. The third section presents the microstructural SEM micrographs representing the particle distribution in various percentages of composites and interface of matrix and reinforcement. In addition wear experimental results followed by Taguchi, ANOVA, and regression analysis and the wear performance of composite and various wear mechanisms. The fourth section depicts the simulation results by using WOA and comparison with other algorithms like PSO, DE, and FFA. The conclusion part is described in the fifth section.

## 2. Experimental Details

### 2.1 Materials and Processing

This section describes the materials consideration and manufacturing of composites with various properties of composites. Composites are fabricated with AZ31 magnesium alloy reinforced with SiC at various percentages of 1%, 2%, 3%, and 4% by using the stir casting method. The flux of 1 wt.% of the matrix (15 wt.% $CaF_2$, 15 wt.% MgO, 20 wt.% KCl, and 50 wt.% $MgCl_2$) is used to avoid oxidation. 10 wt.% of excess AZ31 alloy was in use for the considerations of oxidation losses and slag. The composites are fabricated at $700^0$C at 600 rpm in an argon gas environment, and the homogenization process follows. Then the characterization of the composites is carried out to determine various properties. Table 1 depicts various properties of the AZ31-SiC composites, and the detailed process and methodology were also described (Ref 32).

### 2.2 Microstructure Analysis

The microstructural studies of AZ31-SiC composites at various reinforcements have been carried out using scanning electron microscopy to focus the orientation details of matrix and reinforcement. The distribution of reinforcement particles, the interface details of matrix and reinforcement has been discussed.

### 2.3 Wear Test Experimentation

The ASTM G-99 standard composite specimens of AZ31-SiC are used for conducting experiments on wear testing

**Table 1 Properties of AZ31D -SiC composite**

| Description | 0% | 1% | 2% | 3% | 4% |
|---|---|---|---|---|---|
| Density, g/cc | 1.8 | 1.811 | 1.812 | 1.825 | 1.833 |
| Hardness, HRC | 69.56 | 70.25 | 80.97 | 92.5 | 98.89 |
| Yield strength, MPa | 65.09 | 72.05 | 86.31 | 92.6 | 88.44 |
| Ultimate tensile strength, MPa | 102.30 | 114.56 | 128.07 | 178.4 | 170.71 |
| Compressive strength, MPa | 173.42 | 194.35 | 313.35 | 365.56 | 380.20 |

**Fig. 1** Shows the hunting strategy of WOA

machine (Ducom) to determine the tribological properties. The composite pins are polished with 1200 grit of abrasive and are pressed against the counter body of the EN31 steel disc. The EN31 steel disc is harder than the developed composites, which is supposed to be a dominating factor for forecasting the tribological behavior. The steel disc and pin are cleaned with acetone before each wear test to avoid the presence of non-desirable deposits. The wear tests were conducted for various control parameters of load (10, 15, and 20 N), velocity (0.5, 1 and 1.5 m $s^{-1}$) and sliding distance (500, 750, and 1000 m) with a full factorial design of experiments. The mass loss of the composite was calculated with a micro weighing machine for each wear test. The specific wear rate (mg/mm) of the composite is determined by the weight loss of the pin divided by the sliding distance. Taguchi, ANOVA and Regression analysis was carried out for the wear results. The regression equations for wear and COF generated from regression analysis are used as the objective functions for the optimization of tribological parameters using WOA.

### 2.4 Proposed Whale Optimization Algorithm (WOA)

Whale Optimization Algorithm was developed by Seyedali Mirjalili in the year 2016 (Ref 20). It was developed by observing the hunting method of the Humpback whales. These whales follow a very special hunting method named the bubble net feeding method when searching for their food. The whale makes two paths named as shrinking encircle mechanism (ESM), and spiral mechanism (SM) to reach the target. Figure 1 shows the hunting strategy of WOA. The WOA has been modeled by imbibing these two mechanisms. In this paper, WOA has been used to optimize the tribological parameters of wear and COF.

The procedure for WOA to optimize these values is discussed by using the following steps.

*Step1 Initialization*

The WOA has started with the selection of its parameters to optimize the control variables. The population size of the algorithm and the Number of iterations is considered. The load, speed, and distance have been considered as the tunable parameters. To begin with, all the initial random solutions are generated by using the equation below

$$X_{j_i}^0 = X_j^{\min} + \text{rand}.(X_j^{\min} - X_j^{\max}) \quad \text{(Eq 1)}$$

where $X$ is the tunable parameter, $X_j^{\min}$, $X_j^{\max}$ are the lower and upper bound values of the control variables, $j = 1, 2\ldots N$, where $N$ is the number of control variables, $i = 1, 2,3\ldots\ldots N_p$, $N_p$ is the population size, $rand \in [0, 1]$ is a number that alters between 0 and 1 arbitrarily.

*Step 2 Formulation of an objective function*

The equations obtained from the regression analysis for wear and COF are considered as the objective function for the optimization of control variables.

*Step 3 Search agent updating using SEM (exploration phase)*

The best solution is identified by using WOA. Once fitness function is determined randomly, in the search place, the present best solution is considered as close to the target prey represented in Eq 2 and 3.

$$\vec{S} = \left|\vec{R} \cdot \vec{P^*}(t) - \vec{P}(t)\right| \quad \text{(Eq 2)}$$

$$\vec{P}(t+1) = \vec{P^*}(t) - \vec{A} \cdot \vec{S} \quad \text{(Eq 3)}$$

Here, $\vec{S}$ is used to represent the distance between the prey and the whale. $\vec{R}$, $\vec{A}$ are taken to stand for the coefficient vectors, the letter $t$ stands for the current generation, $P^*$ symbolizes for the best solution obtained so far, $\vec{P}$ represents the position vector, || corresponds to the absolute value, and '.' shows multiplication. The vectors $\vec{A}$, $\vec{R}$ are represented in Eq 4 and 5 as

$$\vec{A} = 2\,\vec{a} \cdot \vec{r} - \vec{a} \quad \text{(Eq 4)}$$

$$\vec{R} = 2 \cdot \vec{r} \quad \text{(Eq 5)}$$

Here $\vec{A}$ stand for a random value varies from 2 to 0 in optimization method and $\vec{r}$ stand for an arbitrary number lies in between (0, 1). The magnitude of $a, A, R$ are changes in each iteration process and are updated in each hunting time. The

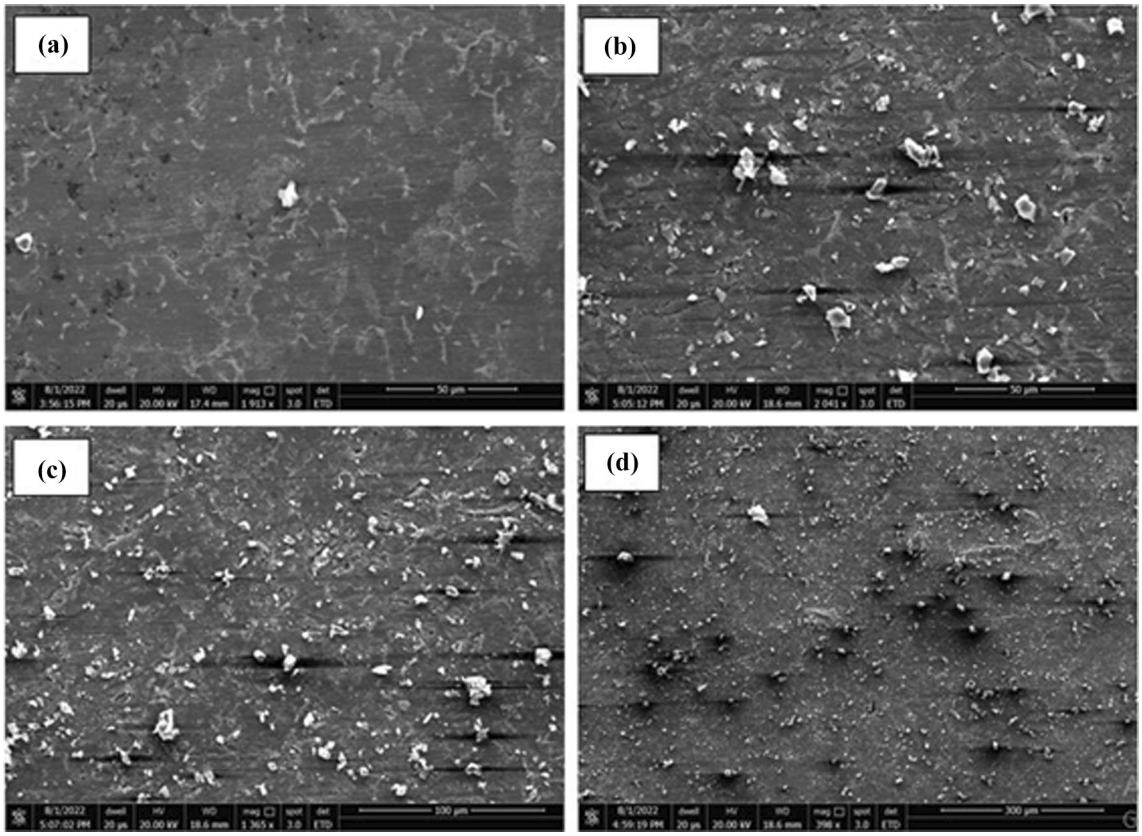


**Fig. 2** SEM images of (a) AZ31D + 1%SiC (b) AZ31D + 2%SiC (c) AZ31D + 3%SiC; (d) AZ31D + 4%SiC

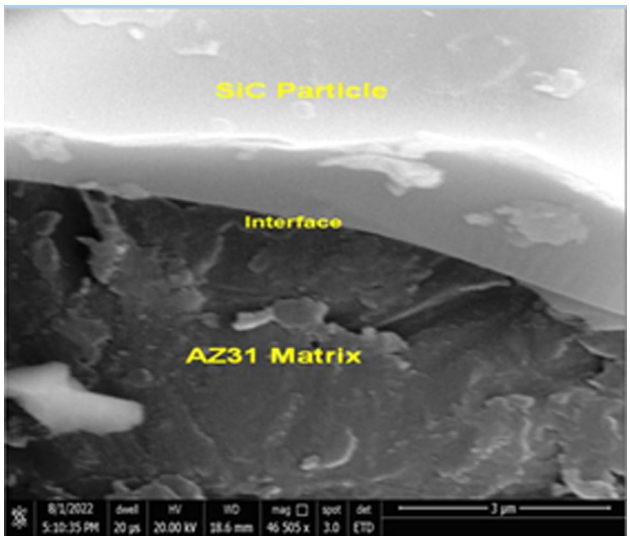


**Fig. 3** SEM image of Interface between AZ31D and SiC

location will be updated by Eq 3 for hunting agents, when the magnitude of $\vec{A}$ is less than 1, and otherwise the following Eq 6 and 7 are considered.

$$\vec{S} = \left|\vec{R} \cdot \vec{P}_{\text{rand}} - \vec{P}\right| \quad \text{(Eq 6)}$$

$$\vec{P}(t+1) = \vec{P^*}(t) - \vec{A} \cdot \vec{S} \quad \text{(Eq 7)}$$

Here $\vec{P}_{\text{rand}}$ represents position of the whale in the population selected randomly.

*Step 4 Updating of searching agent path using SM*

The hunting agent moves in a spiral path to reach the prey. The attack on the target takes place at a time in a shrinking cycle and spiral-shaped path. An equation for spiral shape is formed to simulate the same path between whale and prey. The hunting agent continuously updates its location relayed on Eq 8 and 9.

$$\vec{P}(t+1) = \vec{S}\, e^{bl} \cdot \cos(2\Pi l) + \vec{P^*}(t) - \vec{A} \cdot \vec{S} \quad \text{(Eq 8)}$$

where

$$\vec{S} = \left|\vec{P^*}(t) - \vec{P}(t)\right| \quad \text{(Eq 9)}$$

In this 'l' is a stochastic limit that differs between 0 and 1. Both itineraries are combined together with equal probability to update their location to reach the target. At last, every hunting agent takes the path depicted by Eq 10.

$$\vec{P}(t+1) = \begin{cases} \vec{P} * (t) - \vec{A} \cdot \vec{S} & \text{if } \delta < 0.5 \\ \vec{S}' e^{bl} \cdot \cos(2\Pi l) + \cdot \vec{P} * (t) - \vec{A} \cdot \vec{S} & \text{if } \geq 0.5 \end{cases} \quad \text{(Eq 10)}$$

where $\delta$ is an arbitrary number that varies between 0 and 1.

The flow chart describes various steps involved in the WOA to find the optimal control parameters. It starts with the initialization process, in which all the tunable variables are taken with their minimum and maximum values. Generation of

**Table 2 Wear test results for the full factorial design of experiments**

| S. no. | Load, N | Velocity, m. $s^{-1}$ | Distance, m | Wear, mg | COF |
|---|---|---|---|---|---|
| 1 | 10 | 0.5 | 500 | 4.053 | 0.390 |
| 2 | 10 | 0.5 | 750 | 4.514 | 0.470 |
| 3 | 10 | 0.5 | 1000 | 5.803 | 0.480 |
| 4 | 10 | 1 | 500 | 3.777 | 0.380 |
| 5 | 10 | 1 | 750 | 4.237 | 0.420 |
| 6 | 10 | 1 | 1000 | 4.974 | 0.450 |
| 7 | 10 | 1.5 | 500 | 3.961 | 0.330 |
| 8 | 10 | 1.5 | 750 | 3.869 | 0.390 |
| 9 | 10 | 1.5 | 1000 | 5.159 | 0.460 |
| 10 | 15 | 0.5 | 500 | 4.974 | 0.467 |
| 11 | 15 | 0.5 | 750 | 5.896 | 0.493 |
| 12 | 15 | 0.5 | 1000 | 6.356 | 0.473 |
| 13 | 15 | 1 | 500 | 4.882 | 0.440 |
| 14 | 15 | 1 | 750 | 5.619 | 0.460 |
| 15 | 15 | 1 | 1000 | 5.896 | 0.487 |
| 16 | 15 | 1.5 | 500 | 4.698 | 0.433 |
| 17 | 15 | 1.5 | 750 | 4.974 | 0.453 |
| 18 | 15 | 1.5 | 1000 | 5.619 | 0.473 |
| 19 | 20 | 0.5 | 500 | 5.435 | 0.490 |
| 20 | 20 | 0.5 | 750 | 5.988 | 0.510 |
| 21 | 20 | 0.5 | 1000 | 7.185 | 0.530 |
| 22 | 20 | 1 | 500 | 4.974 | 0.470 |
| 23 | 20 | 1 | 750 | 5.435 | 0.495 |
| 24 | 20 | 1 | 1000 | 6.54 | 0.505 |
| 25 | 20 | 1.5 | 500 | 4.514 | 0.485 |
| 26 | 20 | 1.5 | 750 | 4.882 | 0.465 |
| 27 | 20 | 1.5 | 1000 | 6.264 | 0.490 |

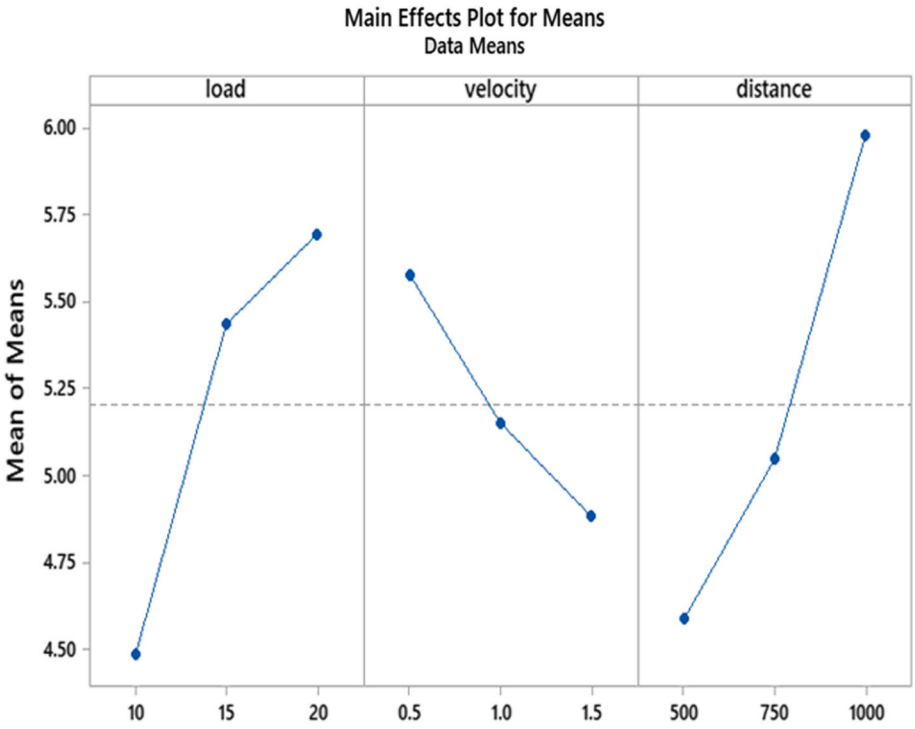


**Fig. 4** Main effects plot for data means of wear

initial solutions, determination of the objective function, and optimization of the tunable parameters according to the mechanisms mentioned above are mentioned in the flowchart. Here, the algorithm will bring to an end when the number of generations is completed. The WOA has been used several times until the optimized parameters are obtained.

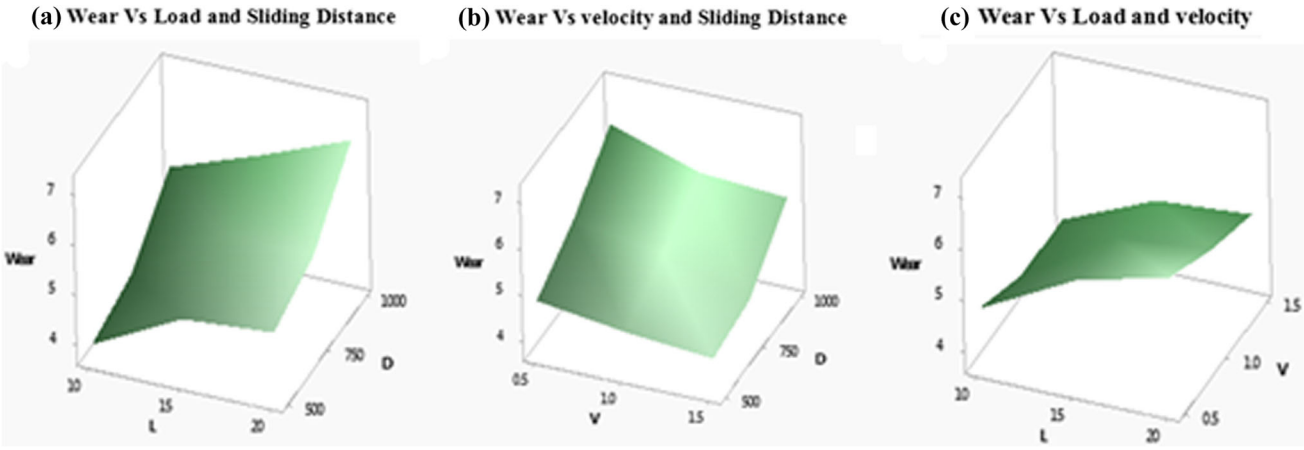


**Fig. 5** Surface plots for wear

**Table 3 ANOVA results for wear**

| Source | DF | SS | MS | F | *P*-value | Contribution, % | |
|---|---|---|---|---|---|---|---|
| Wear | | | | | | | |
| Load(L) | 2 | 7.291 | 3.64545 | 59.17 | 0.000 | 36.83 | Significant |
| Velocity(V) | 2 | 2.220 | 1.11011 | 18.02 | 0.000 | 11.21 | Significant |
| Distance(D) | 2 | 9.052 | 4.52589 | 73.47 | 0.000 | 45.72 | Significant |
| Error | 20 | 1.232 | 0.06161 | | | 6.22 | |
| Total | 26 | 19.795 | | | | 100.00 | |

DF, Degrees of freedom; SS, Sum of squares; Adj SS, Adjusted sum of squares; F-value, Fisher value

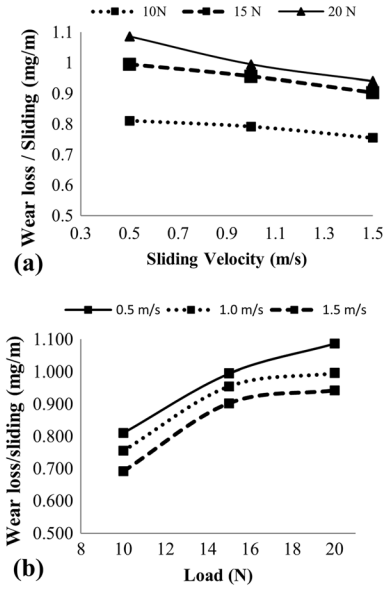


**Fig. 6** Mass loss per sliding (a) as a function of sliding velocity (b) as a function of load

## 3. Experimental Results

### 3.1 SEM Analysis

The microstructural studies of AZ31-SiC composites at various reinforcements are carried out by using scanning electron microscopy are shown in Fig. 2. The SEM micrograph of AZ31 alloy with SiC reinforcement at 1, 2, 3, and 4% are presented in Fig. 2(a)-(d) respectively. The Fig. 3 represents the interface of AZ31 matrix and SiC reinforcement. The inter dendrite regions (IDR's) with SiC reinforced particles, were acknowledged in the composites with uniform distribution. There are no agglomerated particles in the microstructure of the composite due to the uniform distribution of SiC reinforcement. Furthermore, the crack free surface was observed in the interface between matrix alloy and reinforcement (Fig. 3).

### 3.2 Tribological Performance of AZ31/SiC composite

The wear test experiments for wear and COF for various loading conditions of load, speed, and sliding distance were conducted based on full factorial design of experiments and the results are presented in Table 2. The experimental investigation of the composite demonstrates that the minimum wear is noticed at a load of 10 N. The wear increases with the load increases due to deep penetration resulting in a higher material removal rate depicted in Fig. 4. The wear is proportional to the sliding distance, load and inversely with the velocity are presented with surface plots of Fig. 5. The COF of the composite also increased with distance and load due to the higher frictional force generated at the interface. ANOVA is used to study the effect of discrete process factors using MINITAB software. The ANOVA analysis was employed at a confidence interval of 0.95 or a p value of 0.05. It implies that, p value resulted for any parameter $\leq$ 0.05 is significant. The conformity of significance of individual parameter was accomplished with the aid of main effects plot. The results of Table 3 reveal that the highest contributing parameter for wear is the distance of 45.72%, followed by a load of 36.83% & 11.21% of velocity and the highest contributing parameter for COF is the distance of 52.13%, followed by a load of 27.52% &

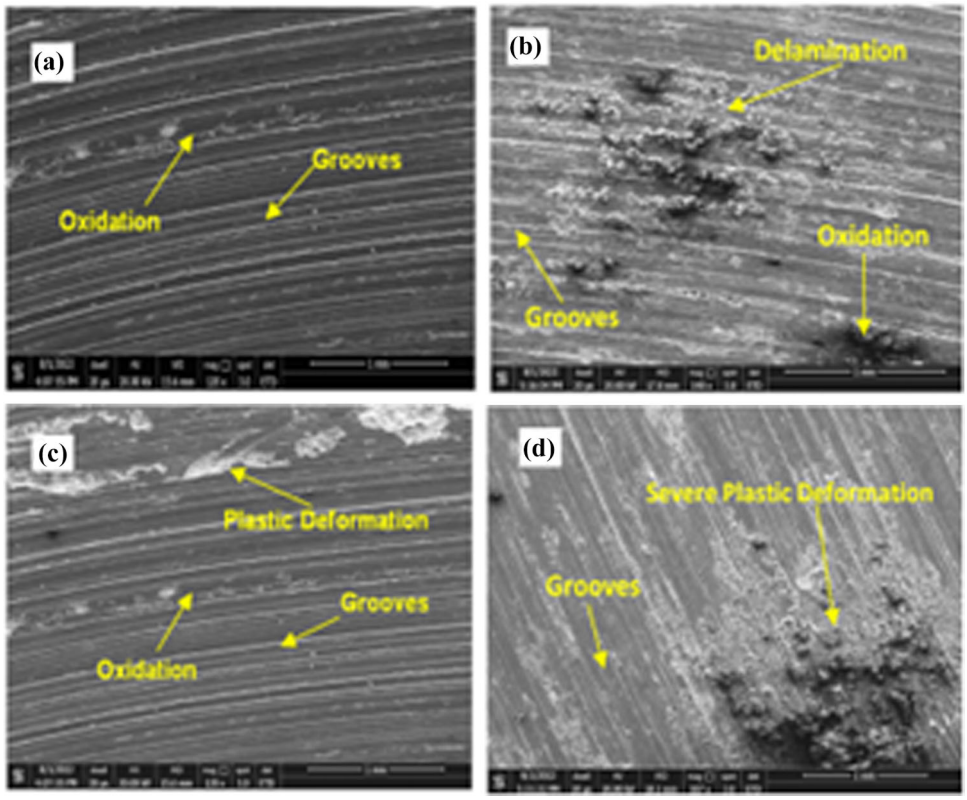


**Fig. 7** SEM micrograph of the AZ31 pins tested at: (a) 20 N, 1.5 m $s^{-1}$ and 1000 m (b) 20 N, 0.5 m $s^{-1}$ and 1000 m (c) 15 N, 1.5 m $s^{-1}$ and 750 m (d) 10 N, 0.5 m $s^{-1}$ and 1000 m

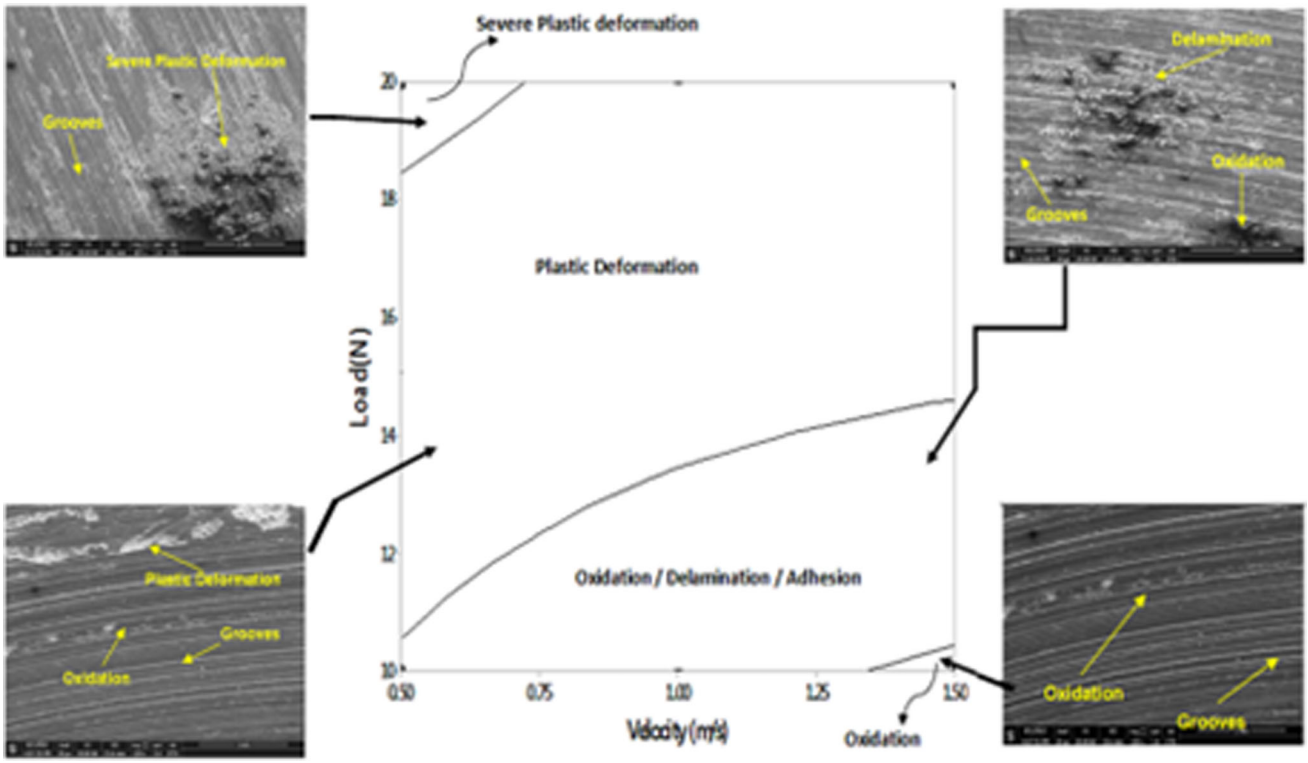


**Fig. 8** Wear mechanism map of the AZ31-SiC with main wear mechanism and different zones

**Table 4 Parameters chosen for whale optimization algorithm**

| Algorithm | Parameters | Values |
|---|---|---|
| Whale optimization algorithm (WOA) | Population size *N* | 100 |
| | Number of iterations | 200 |
| | Constant, *a* | 0-2 |
| Particle spam optimization (PSO) | Population size *N* | 100 |
| | Acceleration coefficients *C1,C2* | 2,2 |
| | Range of weighting factor, *W* | 0.9-0.4 |
| | Number of iterations | 200 |
| Differential evolution (DE) | Population size *N* | 100 |
| | Number of iterations | 200 |
| | Mutation constant *(F)* | 0.5 |
| | Cross over constant *(C.R)* | 0.8 |
| Fire-fly Algorithm (FFA) | Population size *N* | 100 |
| | Number of iterations | 200 |
| | Cooling factor ($\delta$) | 0.97 |
| | Randomization factor ($\alpha$) | 0.2 |

9.41% of velocity. The regression equation for wear rate is obtained for the corresponding $R^2$, $R^2$-Adjusted values of 94.18% and 92.43% and for COF is obtained for the corresponding $R^2$ and $R^2$-Adjusted values of 89.03% and 86.74%. The obtained regression equations are shown in Eq 11 and 12. The R-coefficient values are close to each other, which indicate that the relations between experimental parameters were well predicted and are significant. The values of interaction terms and higher-order terms are close to zero and hence the model becomes linear.

$$Wear = 2.021 + 0.1341L - 0.829V + 0.002606D \quad \text{(Eq 11)}$$

R-sq = 94.18%, R-sq(adj) = 92.43%,

$$CoF = 0.2861 + 0.007662L - 0.03393V + 0.000121D \quad \text{(Eq 12)}$$

R-sq = 89.03%, R-sq(adj) = 86.74%

where L—Load, V—velocity, D—sliding distance

The wear is proportional to the sliding distance, load and inversely with the velocity are presented with surface plots of Fig. 5. For a constant sliding distance, with increase in load wear increases and with increase in velocity wear decreases. For a constant velocity, with increase in load and sliding distance, wear increases. Similar trend is followed for COF. The mass loss per sliding as a function of velocity for the various loads applied is shown in Fig. 6(a). Regardless of the applied force, the lowest sliding velocity (0.5 m $s^{-1}$) produced the maximum mass loss/sliding values. When the sliding velocity is increased, the mass loss per sliding is reduced. For the varied sliding velocities, Fig. 6(b) depicts the mass loss/sliding as a function of the applied load. The sliding velocity of 0.5 m $s^{-1}$ resulted in the greatest mass loss. At all evaluated speeds, the mass loss/sliding increased with the applied load.

### 3.3 Analysis of Worn Surfaces

SEM was used to examine the worn surfaces of the composite test pins in order to identify the primary wear mechanisms that occurred under the various wear conditions investigated (Ref 33, 34). Although numerous wear mechanisms occurred in most of the wear-test situations, a definition of the dominating wear mechanism for each wear test was produced. Abrasion, adhesion, and oxidation were the main wear mechanisms found, as stated below.

Figure 7(a) shows the worn surface of pins tested at 20 N, 1.5 m $s^{-1}$, 1000 m, load, speed, and sliding distance respectively. Adhesion wear mechanism formed due to the joining of metal on pin and metal on the disc at a micro-level. As a result, the material from the pin has been removed and leaves with a disc by creating a void on the pin surface, during the sliding movement. Figure 7(a) depicts the proof of the adhesion wear on the worn-out surface. In addition, the adhesion is preferentially located in the oxidized zone. As result, the adhesion wear mechanism is expected to appear associated with the oxidation wear mechanism. Figure 7(b) shows the worn surface tested at 20 N, 0.5 m $s^{-1}$, and 1000 m load, speed, and sliding distance respectively with oxidation zones, grooves, and abrasive micro-cutting, small delamination zone. Figure 7(c) depicts an increase in the intensity of the groove, plastic deformation zones and oxidation zone on the surface at 15 N, 1.5 m $s^{-1}$, and 750 m. Figure 7(d) depicts the formation of oxide zone with severe plastic deformation and grooves in the direction of sliding at 10 N, 0.5 m $s^{-1}$, and 1000 m. The abrasion wear mechanism causes fine grooves and small oxidation zones are located in the sliding direction, caused due to the presence of hard particles at the interface of contact surfaces. Wear grooves on the surface are formed at low speed along with the oxidation zones. The oxide zones detected on the surface were increased and are ready to detach from the surface. However, low wear rates were observed because of the small size of the oxides formed. The coefficient of friction has been increased due to the detached oxide surfaces. The entire concepts were incorporated in the wear mechanism map for AZ31 magnesium alloy constructed with the relationship of wear rate, coefficient of friction, surface oxidation behavior, and microstructure observation through SEM of the worn surface has to be established as a function of parameters of load and velocity. The load range of 10-20 N and speed range of 0.5-1.5 m $s^{-1}$ are considered for the construction and also represented in various zones depicted in Fig. 8.

## 4. Simulation Results

The Eq 11 and 12 obtained from the regression analysis for wear and COF are considered the objective functions for optimising tribological parameters. The WOA has been developed by considering these objective functions. The design parameters considered for the WOA are depicted in Table 4. The population size is selected as 100, the maximum number of iterations is chosen as 200, and the range value of 'a' is fixed as 0-2. Here, the control parameters of load, speed, and sliding distance are considered for the optimization of tribological parameters. The range of control parameters chosen for the optimization are load (L) of 10-20 N, velocity (V) of 0.5-1.5 m $s^{-1}$, and sliding distance (D) of 500-1000 m respectively. The WOA has been run several times until optimum values have arrived. The design parameters considered for PSO are population size (N) 100, the number of iterations 200, acceleration coefficients ($c_1$, $c_2$) equal to 2, and the range of weighting factor (W) is 0.4-0.9. The design parameters considered for DE are population size (N) of 100, the number of iterations

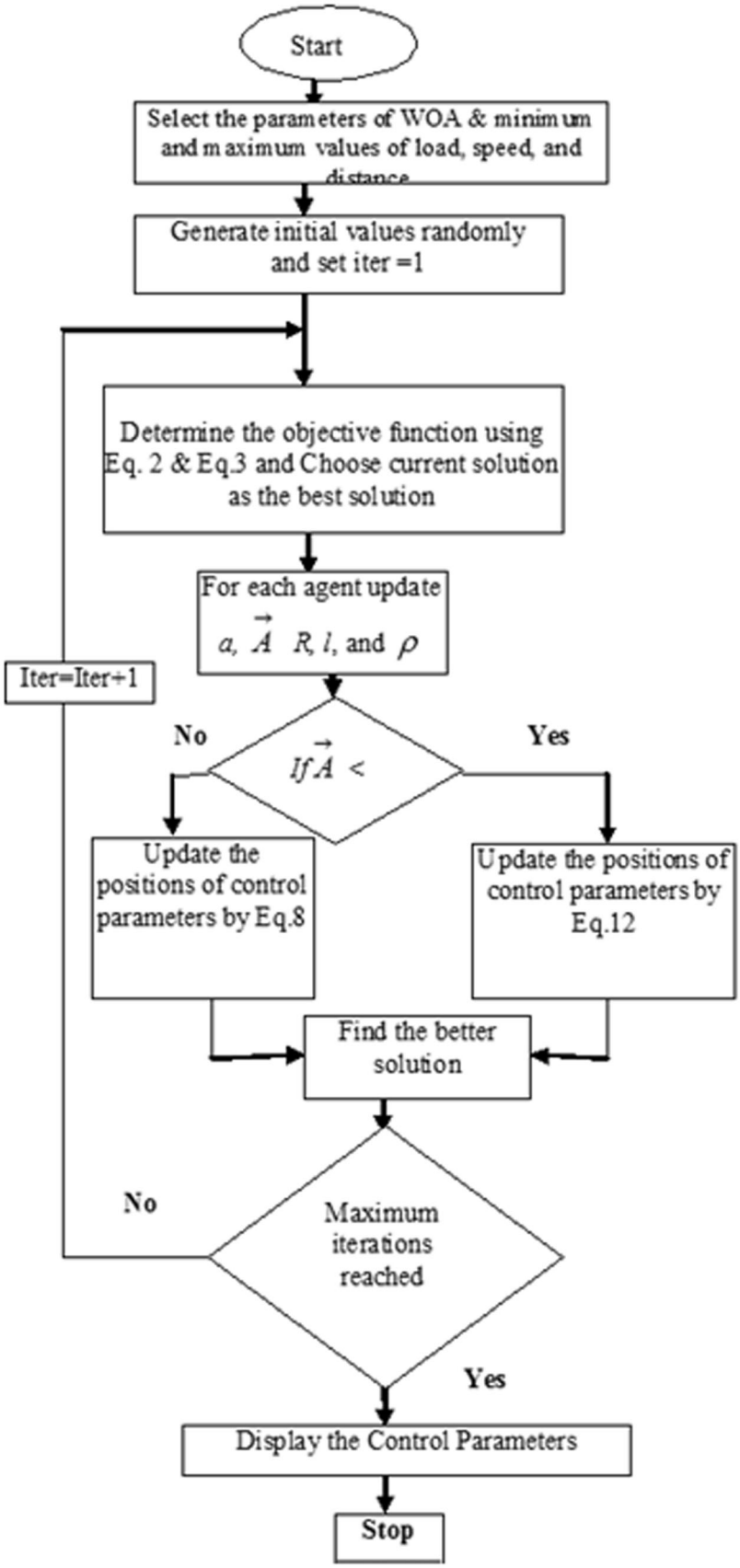


**Fig. 9** Flowchart for WOA to optimize the control parameters

**Table 5 Comparison of results for wear**

| | Wear | | Coefficient of friction | |
|---|---|---|---|---|
| #Algorithm# | Optimum levels | Function value, mg | Optimum levels | Function value |
| WOA | 10 N, 1.489 m $s^{-1}$, 451.5 m | 3.55 | 10 N, 1.492 m $s^{-1}$, 492.5 m | 0.311 |
| PSO | 10.85 N, 1.455 m $s^{-1}$, 483.5 m | 3.62 | 10.75 N, 1.48 m $s^{-1}$, 445.5 m | 0.313 |
| DE | 10 N, 1.48 m $s^{-1}$, 475.5 m | 3.59 | 10 N, 1.475 m $s^{-1}$, 490.5 m | 0.314 |
| FFA | 10 N, 1.42 m $s^{-1}$, 465.5 m | 3.58 | 10 N, 1.487 m $s^{-1}$, 487.5 m | 0.312 |

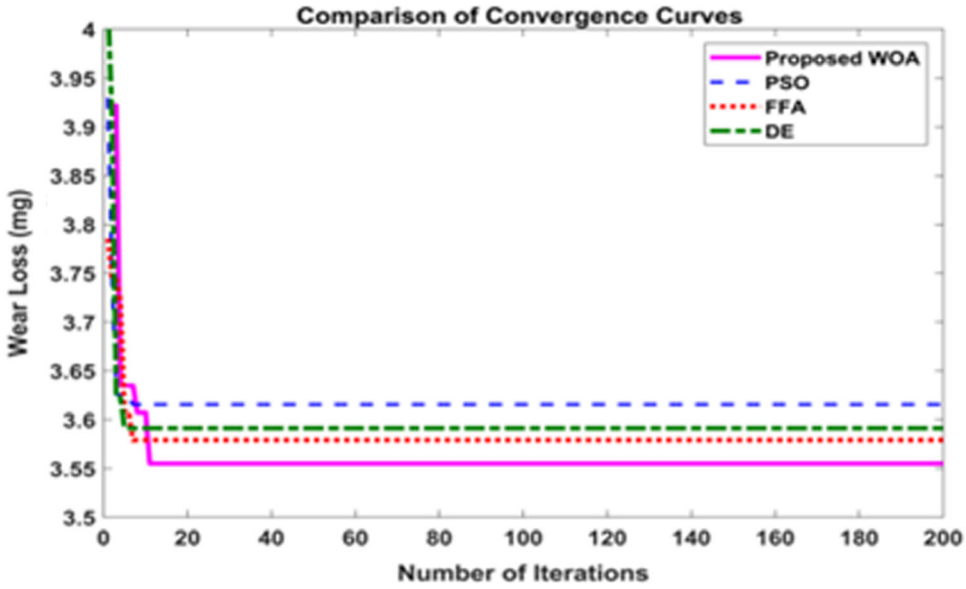


**Fig. 10** Convergence comparison plot for wear using WOA, PSO, FFA, DE algorithms

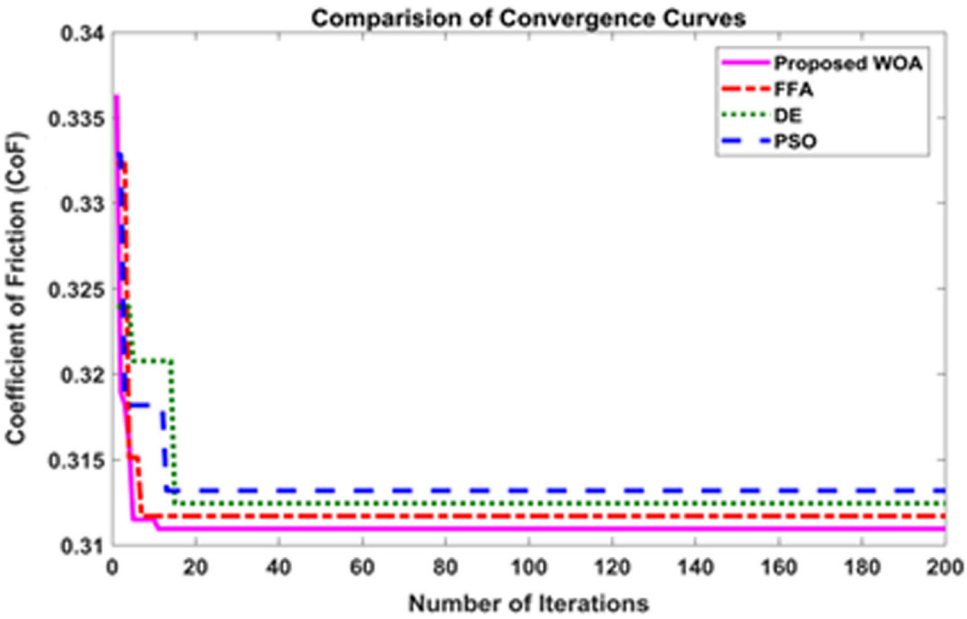


**Fig. 11** Convergence comparison plot for COF using WOA, PSO, FFA, DE algorithms

of 200, mutation constant (F) of 0.5, and cross over constant (C.R) of 0.8. The design parameters considered for FFA are the population size (N) of 100, the number of iterations (200), the cooling factor (δ) of 0.97, and the randomization factor (α) of 0.2. The flowchart for the WOA to evolve the control parameters is depicted in Fig. 9.

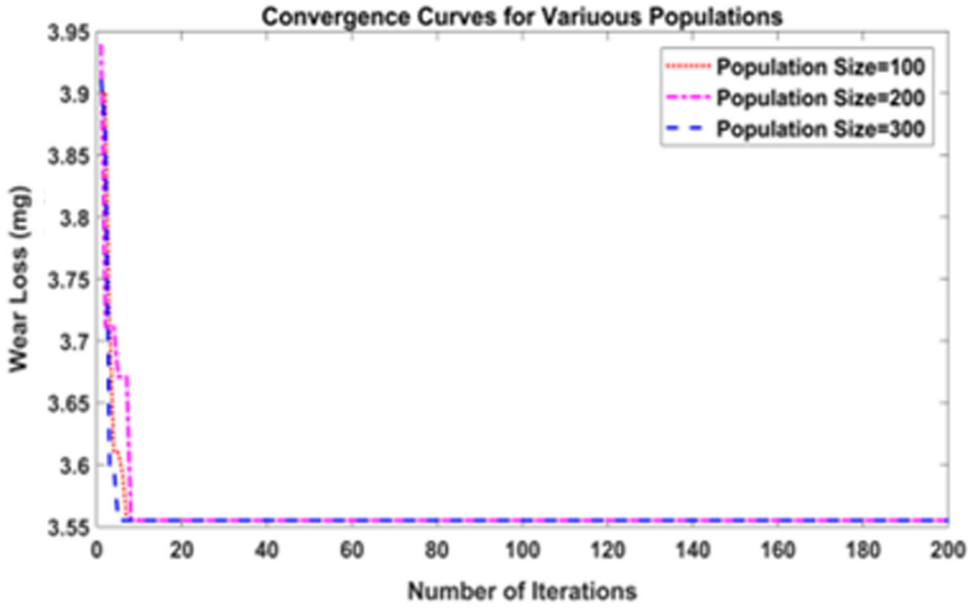


**Fig. 12** Convergence plot for wear with various populations using WOA

The Whale Optimization Algorithm (WOA) has number of advantages over the other algorithms. The biggest advantage of the WOA is that the number of deign parameters for the optimization process is less when compared to other Particle Spam Optimization (PSO), Differential Evolution(DE), and Fire Fly Algorithms (FFA). In case of WOA, only one design parameter (a) is required for the optimization process (Ref 29). The convergence rate of WOA is superior to the other algorithms. The number of steps required in WOA is less when compared to PSO, DE and FFA. In PSO, after initialization of the design parameters, updating of positions is required and then updating of velocity is required for each particle. In case of DE algorithm, after initialization of design parameters, cross over and mutation steps are required for optimization process. In FFA also takes more number of steps for the optimization process. Moreover, for any optimization algorithm, exploration and exploitation are the two important stages upon which the rate of the convergence of optimal solution depends. The exploration stage is to get global best solution and the exploration stage is required to get local best solution. Achieving a good balance between these two stages is the most challenging job for the optimization algorithm because of the stochastic nature of the algorithm. If any algorithm is succeeded in obtaining a good balance between them, then the algorithm can find the optimum solutions. The WOA has been succeeded in maintaining good balance between the exploitation stage and the exploration stage when compared to other algorithms (Ref 30). Hence, the WOA has been considered to design the parameters of wear and coefficient of friction.

The other parameters used for the WOA are depicted in Table 4. The optimum wear values and COF values obtained from WOA, PSO, DE, and FFA are depicted in Table 5. The performance of the proposed WOA is compared with other algorithms like PSO, DE, and FFA. The comparison convergence plots for wear using WOA, PSO, DE, and FFA are shown in Fig. 10. The comparison convergence plots for COF using WOA, PSO, DE, and FFA are demonstrated in Fig. 11. It is evident from the plots that WOA has provided a minimum fitness value when compared to PSO, DE, and FFA. The convergence plots for wear and COF using WOA under various populations are depicted in Fig. 12 and 13, and all curves are close to each other. The percentage of deviation was calculated for the optimised values obtained from WOA, PSO, DE, and FFA is comparison with the experimental value. These percentages of deviation for wear and COF are presented in Table 6.

The optimum wear and COF responses and corresponding control parameters of load, speed, and sliding distance by using WOA, PSO, DE, and FFA are displayed in Tables 5 and 6 respectively. The optimum wear value obtained from the experimental analysis is 3.777 mg with corresponding control parameters of 10 N, 1.0 m $s^{-1}$, and 500 m, whereas the value of COF is 0.33 and the corresponding control parameters are 10 N, 1.5 m $s^{-1}$, and 500 m. The optimum wear value obtained from WOA is 3.55 mg and the corresponding control parameters are 10 N, 1.489 m $s^{-1}$, and 451.5 m, which is 6% lower than the experimental value, whereas the value of COF is 0.311 and the corresponding control parameters are 10 N, 1.492 m $s^{-1}$, and 492.5 m, which is 5.7% lower than the experimental value. The optimum wear value obtained from the PSO algorithm is 3.63 mg and the corresponding control parameters are 10.85 N, 1.455 m $s^{-1}$, and 483.5 m, which is 3.89% lower than the experimental value, whereas the value of COF is 0.313 and the corresponding control parameters are 10.75 N, 1.48 m $s^{-1}$, and 445.5 m, which is 5.15% lower than the experimental value. There is an increase in function values of wear and COF by using PSO algorithm than the WOA. The optimum wear value obtained from the DE algorithm is 3.6 mg and the corresponding control parameters are 10 N, 1.48 m $s^{-1}$, and 475.5 m, which is 4.69% lower than the experimental value, whereas the value of COF is 0.314 and the corresponding control parameters are 10 N, 1.475 m $s^{-1}$, and 490.5 m, which is 4.85% lower than the experimental value. The optimum function values of wear and COF by using DE are more than the WOA. The optimum wear value obtained from FFA is 3.57 mg and the corresponding control parameters are 10 N, 1.42 m $s^{-1}$, and 465.5 m, which is 5.48% lower than the experimental value, whereas the value of COF is 0.314 and

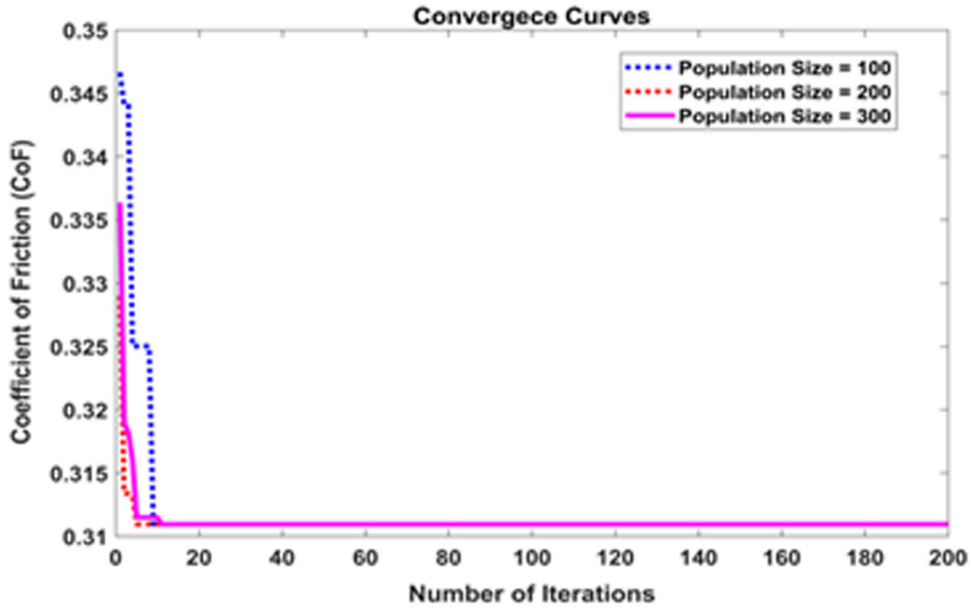


**Fig. 13** Convergence plot for COF with various populations using WOA

**Table 6 Percentage of deviation for wear and COF**

| | Wear | | | Coefficient of friction | | |
|---|---|---|---|---|---|---|
| #Algorithm# | Experimental value, mg | Function value, mg | % of deviation | Experimental value, mg | Function value, mg | % of deviation |
| WOA | 3.77 | 3.55 | 6.01 | 0.33 | 0.311 | 5.76 |
| PSO | 3.77 | 3.63 | 3.89 | 0.33 | 0.313 | 5.15 |
| DE | 3.77 | 3.60 | 4.69 | 0.33 | 0.314 | 4.85 |
| FFA | 3.77 | 3.57 | 5.48 | 0.33 | 0.312 | 5.45 |

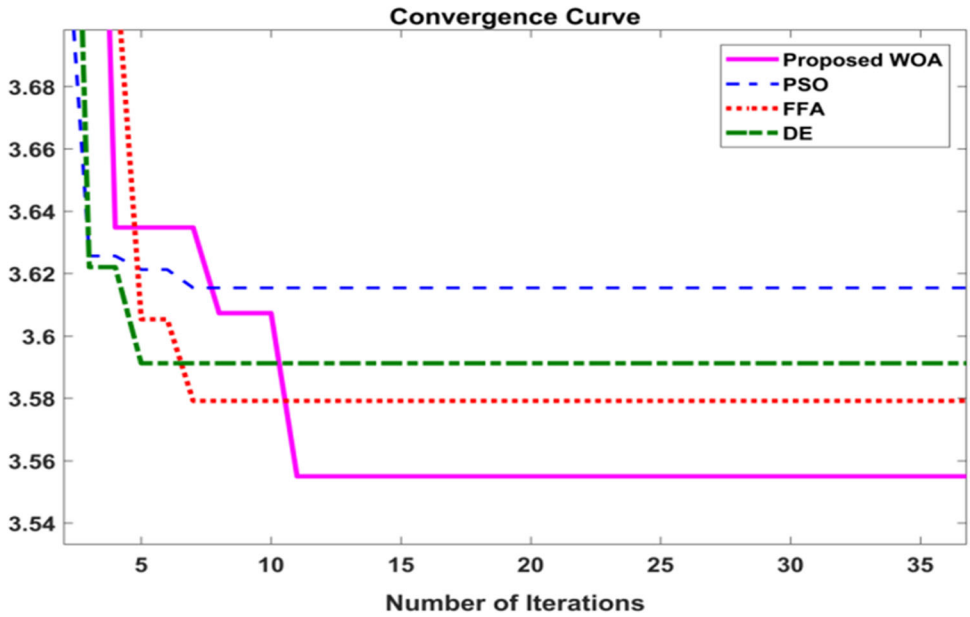


**Fig. 14** Enlarged view of the Convergence zone plot for wear with various populations using WOA

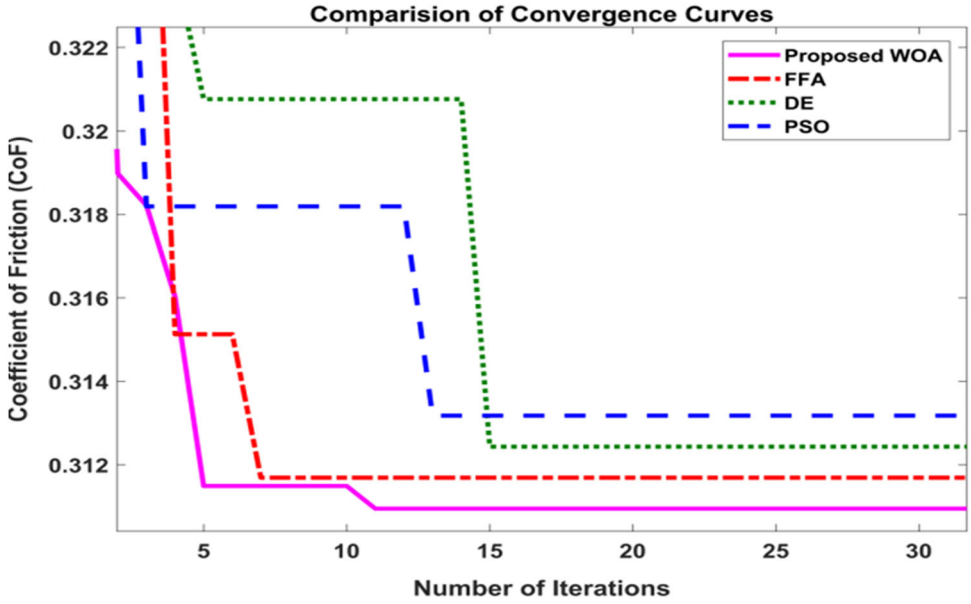


**Fig. 15** Enlarged view of the Convergence zone plot for wear with various populations using WOA

the corresponding control parameters are 10 N, 1.487 m $s^{-1}$, and 487.5 m, which is 5.45% lower than the experimental value. The optimum function values of wear and COF by using FFA are more than WOA. From these simulation results, it is evident that WOA has provided the best results when compared to other algorithms for optimum wear and COF values.

Figure 14 and 15 depict the enlarged view of the comparison convergence plots for wear and COF using WOA, PSO, DE, and FFA respectively. Figure 14 reveals the WOA convergence starts at a wear value of 3.64 mg with 4 iterations and reached to 3.61 mg in one step at 8 iterations and finally reached to 3.55 mg in 11 iterations. The PSO convergence starts at a wear value of 3.63 mg with 2 iterations and finally reached to 3.62 mg in one step at 7 iterations. The DE convergence starts at a wear value of 3.62 mg with 2 iterations and finally reached to 3.59 mg in one step at 5 iterations. The FFA convergence starts at a wear value of 3.61 mg with 2 iterations and finally reached to 3.58 mg in one step at 7 iterations. Figure 15 reveals the WOA convergence starts at a COF value of 0.319 with 4 iterations and reached to 0.312 in one step at 5 iterations and finally reached to 0.311 in 11 iterations. The PSO convergence starts at a COF value of 0.318 with 2 iterations and finally reached to 0.313 in one step at 12 iterations. The DE convergence starts at a COF value of 0.321 with 5 iterations and finally reached to 0.313 in one step at 15 iterations. The FFA convergence starts at a COF value of 0.315 with 4 iterations and finally reached to 0.312 in one step at 7 iterations.

## 5. Conclusions

In this paper, the tribological parameters of AZ31 alloy reinforced with SiC metal matrix composites are optimized using WOA. The WOA has been proposed to optimize the tribological parameters in order to increase the life span of the composite materials with minimum wear and COF. The regression analysis has been carried out by taking the wear test results to frame the equations that are considered to construct the objective functions. These regression equations are the objective functions for the WOA for optimisation. Extensive simulation results are obtained to investigate the efficacy of the proposed WOA. The strength of the WOA is evident by comparing it with the experimental values and other algorithms like FFA, DE, and PSO. From the simulation results, it is concluded that WOA has given global optimum solutions when compared to other techniques. This proposed method reduces the time and effort for the manufacturer to use the composite material in an application with the optimum operating conditions for more life.

## References


1. S. Jayasathyakawin, M. Ravichandran, N. Baskar, C.A. Chairman, and R. Balasundaram, Mechanical Properties and Applications of Magnesium Alloy - Review, *Mater. Today Proc.*, 2020, **27**(2), p 909–913
2. Wojtas M, Sobieszek A, Czajkowski Ł, and Żurawski R. in *Modern Materials in Aerospace Industry—Fatigue Tests of Magnesium Alloy Control System Lever of the Unmanned Ilx—27*. 30th Congress of the International Council of the Aeronautical Sciences, Daejeon, Korea, 25–30.09.2016 (2016). p. 1–7
3. D. Sameer Kumar, C. Tara Sasanka, K. Ravindra, and K.N.S. Suman, Magnesium and its Alloys in Automotive Applications–A Review, *Am. J. Mater. Sci.*, 2015, **4**(1), p 12–30
4. X. Yang, Y. Huang, N.S. Barekar, S. Das, I.C. Stone, and Z. Fan, High Shear Dispersion Technology Prior to Twin Roll Casting for High Performance Magnesium/SiCp Metal Matrixcomposite Strip Fabrication, *Compos. A Appl. Sci. Manuf.*, 2016, **90**, p 349–358
5. P.P. Seth, Om. Parkash, and D. Kumar, Structure and Mechanical Behavior of In Situ Developed Mg2 Si Phase in Magnesium and Aluminum Alloys – A Review, *RSC Adv.*, 2020, **10**, p 37327–37345
6. L. Chen, Y. Zhao, H. Hou, T. Zhang, J. Liang, and M. Li, Development of AZ91D Magnesium Alloy-Graphene Nanoplatelets Composites Using Thixomolding Process, *J. Alloys Compd.*, 2019, **778**, p 359–374
7. R. Yadav, R.K. Gupta, and A. Goyal, Study of Tribological Behaviour of Hybrid Metal Matrix Composites Prepared by Stir Casting Method, *Mater. Today Proc.*, 2020, **28**, p 2218–2222
8. S.C. Sharma, B. Anand, and M. Krishna, Evaluation of Sliding Wear Behaviour of Feldspar Particle-Reinforced Magnesium Alloy Composites, *Wear*, 2000, **241**(1), p 33–40

9. F. Labib, H.M. Ghasemi, and R. Mahmudi, Dry Tribological Behavior of Mg/SiCp Composites at Room and Elevated Temperatures, *Wear*, 2016, **348–349**, p 69–79
10. Q.B. Nguyen, Y.H.M. Sim, M. Gupta, and C.Y.H. Lim, Tribology Characteristics of Magnesium Alloy AZ31B and its Composites, *Tribol. Int.*, 2015, **82**, p 464–471
11. C. Taltavull, B. Torres, A.J. Lopez, and J. Rams, Dry sliding Wear Behavior of AM60B Magnesium Alloy, *Wear*, 2013, **301**, p 615–625
12. C. Taltavull, P. Rodrigo, B. Torres, A.J. Lopez, and J. Rams, Dry Sliding Wear Behavior of AM50B Magnesium Alloy, *Mater. Des.*, 2014, **56**, p 549–556
13. S. Anbu Selvan and S. Ramanathan, Dry Sliding Wear Behavior of Hot Extruded ZE41A Magnesium Alloy, *Mater. Sci. Eng. A*, 2010, **527**, p 1815–1820
14. S. Mingjie, Z. Xiaoqian, H. Baojian, Y. Tao, and J. Junhong, Dry Sliding Wear Behaviour of AZ31 Magnesium Alloy Strengthened by Nano Scale SiCp, *J. Mater. Res. Technol.*, 2022, **16**, p 814–823
15. S.J. Huang, Y.R. Jeng, V.I. Semenov, and Y.Z. Dai, Particle Size Effects of Silicon Carbide on Wear Behavior of SiCp-Reinforced Magnesium Matrix Composites, *Tribol. Lett.*, 2011, **42**, p 79–87
16. S. Ghalme, A. Mankar, and Y. Bhalerao, Integrated Taguchi-Simulated Annealing (SA) Approach for Analyzing Wear Behaviour of Silicon Nitride, *J. Appl. Res. Technol.*, 2018, **15**, p 624–632
17. M. Chen and D.M. Tsai, A Simulated Annealing Approach for Optimization of Multi-Pass Turning Operations, *Int. J. Prod. Res.*, 2007, **34**, p 2803–2825
18. S. Mirjalili, The Ant Lion Optimizer, *Adv. Eng. Softw.*, 2015, **83**, p 80–98
19. A.G. Joshi, M. Manjaiah, and S. Basavarajappa et al., Wear Performance Optimization of SiC-Gr Reinforced Al Hybrid Metal Matrix Composites Using Integrated Regression-Antlion Algorithm, *SILICON*, 2020, **13**, p 3941–3951
20. S. Mirjalili, P. Jangir, and S. Saremi, Multi-Objective Ant Lion Optimizer: a Multi-Objective Optimization Algorithm for Solving Engineering Problems, *Appl. Intell.*, 2017, **46**, p 79–95
21. M.O. Shabani and A. Mazahery, Application of GA to Optimize the Process Conditions of Al Matrix Nano-Composites, *Compos. B Eng.*, 2013, **45**(1), p 185–191
22. E.S. Barroso, E. Parente, and A.M. Cartaxo de Melo, A Hybrid PSO-GA Algorithm for Optimization of Laminated Composites, *Struct. Multidisc. Optim.*, 2017, **55**, p 2111–2130
23. C. Liu, W. Ding, and Z. Li et al., Prediction of High-Speed Grinding Temperature of Titanium Matrix Composites Using BP Neural Network Based on PSO Algorithm, *Int. J. Adv. Manuf. Technol.*, 2017, **89**, p 2277–2285
24. V.N. Gaitonde, S.R. Karnik, and J.P. Davim, *Computational Methods and Optimization in Machining of Metal Matrix Composites*, Springer, London, 2012
25. T.P. Dao, S.C. Huang, and N. Le Chau, Robust Parameter Design for a Compliant Micro Gripper Based on Hybrid Taguchi-Differential Evolution Algorithm, *Microsyst. Technol.*, 2018, **24**, p 1461–1477
26. U. Esme, K.K. Mustafa, U. Deniz, B. Barış, K. Yigit, and O. Seref, Modeling and Optimization of CNC Milling of AISI 1050 Steel by a Regression Based Differential Evolution Algorithm (DEA), *J. Mater. Test.*, 2018, **58**, p 632–639
27. T. Srichok, R. Pitakaso, K. Sethanan, W. Sirirak, and P. Kwangmuang, Combined Response Surface Method and Modified Differential Evolution for Parameter Optimization of Friction Stir Welding, *Processes*, 2020, **8**(9), p 1080
28. X.S. Yang, Firefly Algorithm, Stochastic Test Functions and Design Optimisation, *Int. J. Bio-Inspir. Comput.*, 2010, **2**(2), p 78–84
29. B. Dasu, M. Siva Kumar, and R. Srinivasa Rao, Interconnected Multi-Machine Power System Stabilizer Design Using Whale Optimization Algorithm, *Prot. Control Mod.*, 2019, **4**(2), p 3574
30. B. Dasu, M. Siva Kumar and R. Srinivasa Rao, An Improved Whale Optimization Algorithm for the Design of Multi Machine Power System Stabilizer, *Int. Trans. Electr. Energy Syst.*, 2020, **30**(5), p e12314
31. B. Dasu, M. Siva Kumar, and R. Srinivasa Rao, Model Order Reduction Based Power System Stabilizer Design Using Improved Whale Optimization Algorithm. IETE J. Res., 1–20 (2020)
32. K.C. Kumar, B.R. Kumar, and N.M. Rao, Microstructural, Mechanical Characterization, and Fractography of AZ31/SiC Reinforced Composites by Stir Casting Method, *SILICON*, 2021, **16**, p 1–11
33. I.H. Kara and A. Incesu, Microstructural, Mechanical, and Tribological Properties of Mg-3Al-1Sn-1Nd-Mn Alloy, *J. Mater. Eng. Perform.*, 2021, **30**, p 1674–1682
34. S. Farahany, H. Ghandvar, N.A. Nordin, and A. Ourdjini, Microstructure Characterization, Mechanical, and Tribological Properties of Slow-Cooled Sb-Treated Al-20Mg2Si-Cu In Situ Composites, *J. Mater. Eng. Perform.*, 2017, **26**, p 1685–1700